Study on wavelet entropy for airport pavement inspection using a multi-static GPR system

Zou, Lilong ORCID: https://orcid.org/0000-0002-5109-4866, Kikuta, Kazutaka, Alani, Amir and Sato, Motoyuki (2021) Study on wavelet entropy for airport pavement inspection using a multi-static GPR system. Geophysics. ISSN 0016-8033

http://dx.doi.org/10.1190/geo2020-0361.1

GEOPHYSICS®

Study on Wavelet Entropy for Airport Pavement Inspection using a Multi-Static GPR System

Journal:	*Geophysics*
Manuscript ID	GEO-2020-0361.R3
Manuscript Type:	Shallow Void, Tunnel, and Other Anomaly Detection
Keywords:	common midpoint (CMP), engineering, ground-penetrating radar (GPR)
Manuscript Focus Area:	Engineering and Environmental Geophysics, Ground-Penetrating Radar

ABSTRACT

The multi-layer nature of airport pavement structures is susceptible to the generation of voids at the bonding parts of the structure, which is also called interlayer debonding. Observations have shown that the thickness of the resulting voids is usually at the scale of millimeters, which makes it difficult to inspect. The efficient and accurate characteristics of ground penetrating radar (GPR) make it suitable for large area inspections of airport pavement. In this study, a multi-static GPR system was used to inspect the interlayer debonding of a large area of an airport pavement. A special antenna arrangement can obtain common mid-point (CMP) gathers during a common offset survey. The presence of interlayer debonding affects the phase of the reflection signals, and the phase disturbance can be quantified by wavelet transform. Therefore, an advanced approach that uses the average entropy of the wavelet transform parameters in CMP gathers to detect the interlayer debonding of airport pavement is proposed. The results demonstrate that the regions with high entropy correspond to the regions where tiny voids exist. The new approach introduced in this study was then evaluated by a field-base experiment at an airport taxiway model. The results show that the proposed

17 approach can detect interlayer debonding of the pavement model accurately and efficiently. The on-site coring results confirm the performance of the proposed approach.

INTRODUCTION

Maintaining pavement facilities (runway, taxiway) at the airport faces many unique challenges. A significant amount of economic costs and a large number of airport engineering and maintenance personnel are required to provide all-weather facilities for the safe operation of the airport. The integrity and flatness of airport pavement facilities plays an important role in the safe operation of aircraft. Even a small defect and the resulting debris can cause catastrophic accidents. So, the anomalies must be accurately detected before major damage occurs due to the particular requirements of airport pavement facilities. Hence, it is important to develop a low-cost, reliable and effective detection technology to detect anomalies in the concrete structure of the airport, thus providing integrity and safety services to aircraft operating at airport road facilities (Frederickson and LaPorte, 2002).

~~In order~~ to meet the high standard requirements of perfect flatness, toughness, and uniformity of airport road facilities, multi-layer designs with different materials are usually used for construction (Fwa, 2003). Normally, the multi-layer structure consists of

3 to 4 layers. They are a surface asphalt layer, base asphalt layer, sub-base layer, and bottom layer from the surface to bottom. Typically, the thickness of each layer is about several centimeters (Zou et al., 2018). However, the multi-layer design of airport pavement has its disadvantages. A small raindrop or snow flake on the surface can be pressed into the pavement structure when an aircraft moves over the pavement. This small amount of water can remain in the small area of the shallow pavement. With changes in pavement surface temperature, the volume of water becomes larger (when the temperature is high, it becomes water vapor; when the temperature is low, it turns to ice), expands and extends as a void on the layer bonding region (usually called interlayer debonding phenomenon). At the same time, the temperature and pressure change generated by the aircraft moving over the pavement can further accelerate this procedure. The integrity of the airport pavement becomes weaker as the interlayer debonding extends further and further, and the pavement surface could be distorted and collapse, thus affecting the safe operation of aircraft. The interlayer debonding plays an important role in the remaining life of airport pavement facilities. Therefore, it is important to detect

49 interlayer debonding at its early stage ~~and repair it~~. This is the priority for airport road maintenance.

51 In recent years, non-destructive testing (NDT) has been widely used in airport pavement inspection and maintenance due to the reliable and efficient information that it can provide (Breysse, 2012; Liu et al., 2020). Ground Penetrating Radar (GPR), Infrared Thermal Imaging, Acoustic or Ultra-Sounding Detection, and Microwave Remote Sensing are widely used to detect the inner anomalies of concrete infrastructure. The accuracy and economy of these technologies fully guarantee the integrity and safety of the pavement infrastructure. At present, the conventional methods of anomaly detection in airport pavement facilities are acoustic imaging and infrared irradiation methods. Acoustic imaging needs a large number of experienced engineers and technicians, while infrared radiation cannot be applied to large-scale rapid detection due to the strict conditions and limited size for pavement inspection (Zou, et al., 2020). However, due to the existence of tiny voids, the small density change in the depth direction can be used for inspection. Based on this idea, both nuclear densitometer and ultrasonic measurements have

achieved accurate results in laboratory experiments. But, these two methods are not suitable for real-life application to large-scale inspection of airport pavement.

As an NDT method, GPR can provide optimal resolution of different applications ~~in civil engineering~~ (Alani and Tosti, 2018; Benedetto et al., 2017; Eskelinen and Pellinen, 2018; Liu et al., 2020; Saarenketo and Scullion, 2000; Shangguan et al., 2016; Spagnolini, and Rampa, 1999; Lai et al., 2018) due to the ultra-wide frequency band that is used. For the detection of airport pavement facilities by GPR, the challenge mainly comes from how to extract information from the reflection generated by the small anomalies. This is quite different from the data processing for most pavement inspection cases, which focuses on large-scale anomalies in the deep region of the pavement. Meanwhile, the anomalies inside the structural layers of airport pavement are millimeter order in size (Zou, et al., 2020). These thin layers are difficult to directly observe on the GPR profile given the system resolution, as pointed out by Bradford and Deeds (2006) and Hartikainen et al., (2018). Besides, the thin layers in airport pavement facilities are usually shallow (a few centimeters depth); (Zou, et al., 2020). The complex electromagnetic response generated by the electromagnetic wave at the boundary of air and pavement cannot be separated from the response of small shallow anomalies. How to interpret, from a GPR signal with a center frequency of several GHz, the responses from such small, shallow anomalies has become a difficult task and a challenge. In addition, in the light of the slight dielectric coefficient difference or the change in velocity of the shallow pavement structure due to the presence of tiny voids, GPR measurements have made it possible to further identify the anomalies of the airport pavement. However, the small change of dielectric coefficient does not produce an obvious anomaly by the conventional survey and processing.

Further expanding on the above idea, considering the size, location of the thin layer, and the system resolution, the small change of dielectric coefficient along the horizontal direction can also be used to judge the existence of anomalies in the airport pavement structure. Because this change is extremely small, a reference or level should be considered. The reference or level can be the reflection from a certain point or a multichannel response. Based on the above idea, Yi et al. (2018) proposed an approach

94 that analyzes the tiny deviation of the asphalt layer depth and velocity by using the phase
95 deviation of the common mid-point (CMP) gather for airport pavement inspection. Zou et
96 al. (2020) proposed another method that uses the energy deviation of the lateral wave in
97 a CMP gather for the airport pavement inspection. Both of these methods are verified by
98 real measurements carried on pavement at Tokyo International Airport (Japan). However,
99 due to the difficulty of parameter adjustment, there are some limitations in practical
100 application (Yi et al., 2018; Zou et al., 2020) of the above methods.

101 In this paper, we investigate a new approach, which is robust, easy to understand,
102 and practical in terms of implementation and results. The proposed approach analyzes
103 the average wavelet entropy of the shallow region reflection in a CMP gather. Compared
104 to the Fourier transform, the wavelet transform has many advantages for representing the
105 detailed information in a signal. The wavelet transform can deconstruct and reconstruct
106 any aperiodic signals accurately. It can analyze the localization of time- or space-
107 frequency by stretching and shifting the signal step by step. The detailed information in
108 the signal can be represented by time subdivision at high frequency and frequency

109 subdivision at a low frequency through the wavelet transform (Kumar, and
110 Foufoula-Georgiou, 1997; Sinha et al., 2005). The entropy, which analyzes and
111 compares the probability distribution, can provide a measure of the signal stability.
112 The wavelet entropy, which combines wavelet analysis and entropy, can be used as
113 a measure of the degree of order/disorder of the signal. Therefore, it can provide
114 useful information about signal dynamical stability. In recent years, wavelet entropy as
115 a robust method has been widely applied for fault detection (Rosso et al., 2001; El-
116 Zonkoly and Desouki, 2011; Dasgupta et al., 2012).

117 Due to presence of a thin void or a micro-damaged zone, the waveform of the
118 backward reflection has some slight changes compared to the sound zone. This small
119 change can be illustrated by an entropy change throughout the parameters of the wavelet
120 transformation. So, the proposed approach is based on the wavelet entropy difference
121 between the anomalies and sound pavement reflections. The signal processing
122 procedure for the proposed approach is also succinct. First, a band-pass filter is applied
123 to the raw frequency domain data and then the Fourier transform was performed to get

time-domain CMP gathers. Next, the trace balance of each CMP gather is applied. Trace balance is a procedure that scale amplitudes to a common root mean square (RMS) level ~~for all traces~~. Lastly, the mean wavelet entropy of the shallow region reflection is calculated and formed into a 2D entropy map of the entire measurement area. The simple processing procedure makes the real-time pavement inspection much easier perform. Real experiment data obtained from a pavement model have demonstrated the excellent performance of the proposed approach. The processed results also matched with on-site coring results very well.

MULTI-STATIC GPR SYSTEM AND PAVEMENT MODEL

Multi-static Ground Penetrating Radar System and Survey Strategy

With the further increase of GPR application in civil and environmental engineering, several array radar systems have been developed (Gerhards et al., 2008; Jol, 2008; Xu et al., 2002). To better carry out large-scale measurement, Tohoku University (Japan) developed an array radar system in 2012 (Liu et al., 2013; Sato et al., 2016, Yi et al., 2018; Kikuta et al., 2019), shown in Figure 1. The system consists of 8 bowtie antennas that form the transmitting array and the receiving array as shown in Figure 2. The receiving array and the transmitting array are staggered with a half antenna interval. It is a step frequency continuous wave radar system and the operating frequency varies from 0.05 GHz to 1.5 GHz. The system is a multi-static system which means all the combinations of transmitter and receiver antenna are recorded. Overall, 64 channel data can be obtained by a single measurement. It uses a distance-measuring wheel to trigger and record the data every 0.01 m interval. The system length is 2 m and can cover an area of 2 m at a time. It can be hung on the vehicle and also can be pulled manually. The fastest measuring speed can reach 7km / h. Based on the above advantages, the system can cover a large survey area and acquire a dense GPR dataset in a short time. Table 1 shows the main parameters of the multi-static GPR system. By operating this system, a large-scale GPR survey can be carried out efficiently.

In addition to the advantages described above, CMP gathers can be extracted from the antenna arrangement ~~of this system at the same time~~ during a common measurement. Of course, this cannot be achieved by the common parallel survey, and so an improved survey strategy is needed. By separating the transmitting and receiving antenna by a relatively small distance simultaneously, a series of reflections from the middle point can be obtained. The reflections can be formed as a CMP gather. As shown in Figure 3, a CMP gather can be extracted by judicious choice of traces from the 64 channel data. A point located in the middle of the system can have 8 CMP traces, while the edge point only has 1 trace. Set each parallel survey line interval as 0.84 m and this way can guarantee that each center point has at least 4 CMP trace. Therefore, the dense CMP gathers with a 0.12 m interval along the cross-survey direction, and a 0.01 m interval along the survey direction can be extracted with at least 2 parallel surveys. In this paper, 4 traces with antenna offsets 0.13 m, 0.21 m, 0.32 m, and 0.44 m ~~were used~~ for all ~~the~~ CMP gathers. Although 4 traces in a CMP gather is sparse compared to traditional CMP acquisition, the CMP gathers extracted by this multi-static GPR system still could be used for further signal processing.

Survey Site and Pavement Structures

~~In order~~ to provide adequate support for the frequent operation of aircraft, it is important to construct a sufficiently strong, stable and smooth airport pavement. First, the pavement structure must be of adequate thickness and strength to withstand the loads imposed by the aircraft. Secondly, it must have good wear resistance under frequent operation, and will not produce small debris to affect the safety of the aircraft. Finally, it must also be able to withstand the effects of extreme weather to ensure the safe operation of the aircraft. To find the pavement that meets the above requirements, many factors such as design, construction, and material combinations need to be coordinated to find the best combination.

In order to find the best material combination and to monitor its performance under high loads, a pavement model was built in the Port and Airport Research Institute located in Nobi, Kanagawa, Japan, as shown in Figure 4 (a). The size of this model is 4 m in width and 50 m in length. It is a multi-layer structure consisting of a surface layer, a base layer, and a leveling layer. The structural strength was provided primarily by the surface and the base layers. They can reduce the load stress produced by the aircraft to a degree that is

183 adequately sustained by the subgrade. This model was divided into 7 parts with different
184 kinds of material combinations, as shown in Figure 5. Two side areas are 10 m in length.
185 The middle of this model was divided into 5 zones all 6 m in length. The surface layer and
186 leveling layers are asphalt layers with 0.05 m thickness and 0.04 m thickness,
187 respectively. Figure 6 (a)-(e) show the side view of Area I to Area V. The base layers
188 located in Area I to Area V are gravel (Figure 6 (f)), low-density asphalt, low-density
189 asphalt, high-density asphalt, and high-density asphalt, respectively. The base layers on
190 the side of this model are also high-density asphalt, as shown in Figure 6 (g). The
191 thickness of the base layer is 0.06 m. Under the base layers of Area I, Area II and Area
192 V, nonwoven fabrics were buried. Water tanks were built on the outside of these areas
193 and continuous water injection was performed during the monitoring. Such a design
194 imitates the natural procedure of the interlayer debonding phenomenon of airport
195 pavement. The non-woven fabric can bring water into the layer bonding part to imitate the
196 process of pressing raindrops or snow into the pavement when an aircraft moves over it.
197 After the model was built, a 20-ton truck (Figure 6 (h)) repeatedly ran over the model to
198 imitate the loads imposed by the aircraft for 30 days until November 30th, 2017. Four

GPR surveys were conducted from the initial build to the end of the 30 days load test. The first measurement was performed just after the model was built. The second test was performed after 7 days of loading and injection of water. The third measurement was taken 10 days after the second measurement. And the last measurement was completed by the end of the evaluation.

Three survey lines were designed at 1.08 m, 1.92 m, and 2.76 m in the X-direction. In this way, a large number of CMPs can be collected from 0.6 m to 3.24 m with 0.12 m intervals in the X direction and every 0.01 m in the Y direction. Overall, more than 100 thousand CMP gathers were available for further analysis in this survey area.

SIGNAL PROCESSING

The processing procedure for the proposed approach consists of three sequential stages. Pre-processing algorithms include band-pass filtering and trace balancing of each CMP gather to increase the overall signal to noise ratio. Subsequently, the wavelet transform was performed in the shallow region reflection. In this paper, the asphalt dielectric coefficient is presumed to be 4 and the wavelet analysis was performed using a response signal from 0 to 4 ns. The 4 ns lapse signal is adequate to contain all the reflecting layers compared to the 0.15 m thick pavement model. In the last stage, the entropy value was calculated on the basis of the wavelet coefficients and thus the mean entropy values of each CMP could be obtained. Finally, a 2D mean wavelet entropy map of the entire measurement field is produced for interlayer debonding detection.

The stability of the reflection signal phase is the main point of the proposed approach. Ideally, the reflection of the GPR is a direct function of the coefficient of reflection. But many factors will affect the stability of the reflection at the target boundary. It will make the inspection of anomalies difficult. However, some considerations and assumptions can be assumed to mitigate this impact by considering the airport asphalt pavement properties.

The basic assumption of this proposed approach is that the material itself does not change the reflection phase with the offset. The first assumption is the transmission loss of the asphalt can be assumed as a constant with offset (Shang and Umana, 1999;

Jaselskis et al., 2003). Another assumption is that the asphalt is a frequency-independent material for the operating bandwidth of the GPR system (Lai et al., 2011). It is a basic and reasonable assumption of the proposed approach because it could significantly affect the phase information of different offset reflections.

Mean Wavelet Entropy

Compare to Fourier analysis, wavelet analysis can process a signal with different scales and resolutions. A large window can be applied in wavelet analysis which results in the global features. Similarly, analyzing a signal with a small window can pick out localized features. Based on these characteristics, wavelet analysis has been successfully applied in many applications, such as image analysis, transient signal analysis, and other signal processing applications.

Wavelet is a kind of smooth and fast fading wave, which has good localization both in frequency and time. The wavelet family $\Theta_{a,b}$ is a set of basic functions, which are generated by the expansion and translation of a unique mother wavelet $\Theta(t)$:

$$\Theta_{a,b}(t) = |a|^{-\frac{1}{2}}\Theta\left(\frac{t-b}{a}\right) \tag{1}$$

where t is the time, a indicates the scale parameter, and b indicates the translation parameter. The duration of the wavelet increases with the increase of the scale parameter a. Therefore, wavelet analysis has a unique analysis model, which uses different scales and variable time to analyze the signal.

The continuous wavelet transform (CWT) of a signal $s(t)$ is defined as the correlation between a and b parameters with the family wavelet $\Theta_{a,b}$

$$Coef(a,b;s(t)) = \int_{-\infty}^{\infty} s(t)\frac{1}{a}\Theta\left(\frac{t-b}{a}\right)dt \tag{2}$$

Not only will the selected wavelet affect the coefficients of a CWT, but so will the values of scale and position. The CWT coefficients $Coef(a,b)$ can be obtained by continuously changing the values of scale parameter a and translation parameter b.

Discrete wavelet transform (DWT) provides a non-redundant representation of the signal, and its values constitute the coefficients in the wavelet transform. Wavelet coefficients can provide complete information of signals. Moreover, the local energy can be directly estimated at different scales through the wavelet coefficients. The DWT of a discrete signal $s(n)$ can be derived from CWT and expressed as

$$Coef(m,u;s(n)) = \sum_{n=1}^{N} s(n)\frac{1}{a}\Theta\left(\frac{u - nb_0a_0^m}{a_0^m}\right) \quad (4)$$

where a_0^m indicates the discrete scale parameter and $nb_0a_0^m$ indicates the discrete translation parameter, m indicates the scale parameter and u indicates the translation parameter of the wavelet transform.

Then, the wavelet energy of the analyzed signal can be calculated throughout the wavelet coefficients and expressed as:

$$Energy_m = \sum_k |Coef(m,u)|^2 \quad (5)$$

Finally, the total wavelet energy can be obtained as:

$$Energy_{total} = \sum_m Energy_m \tag{6}$$

Then, the relative wavelet energy ~~can be~~ expressed as:

$$RE_m = \frac{Energy_m}{Energy_{total}} \tag{7}$$

From the above equations, the relative wavelet energy RE_m can be considered as a time-scale density and satisfies the following relationship:

$$\sum_m RE_m = 1 \tag{8}$$

This provides a suitable tool for detecting and characterizing the time and frequency attributes of signals.

According to the relative wavelet energy and the Shannon entropy theory (Zhang et al., 2015), the wavelet entropy is defined and expressed as:

$$S_{WE}(p) = -\sum_m RE_m \cdot \ln(RE_m) \tag{9}$$

A reflected signal coming from the defects or anomalies in the pavement region can be taken as a combination of two signals. One signal is the reflection comeing from the sound pavement. The other signal is a difference signal between the signals that come from the defective and sound pavement. This type of reflection will have its form of wavelet representation and will have an important contribution to all frequency bands. As a result, the relative wavelet energy of all resolution levels will be almost equal, and the wavelet entropy will exceed the maximum value. In addition, this signal can also break the stability of each CMP trace.

In this study, the wavelet analysis of shallow region reflection was performed by equation (4) and the wavelet coefficients were obtained. Then the relative wavelet energy was obtained by equations (5) to (7). Next, the wavelet entropy of each CMP trace was calculated by equation (9). Finally, the mean wavelet entropy of a CMP gather can be obtained according to each CMP trace entropy value.

RESULTS AND DISCUSSIONS

Field Measurement Results

In this study, the test was carried from October 30th to November 30th, 2017. Four GPR surveys were conducted from the initial build to the 30 days load test and water injection. The first measurement was conducted on October 30th. The second measurement was conducted on November 6th. The third measurement was conducted on November 14th. And the last measurement was conducted on November 30th.

Three survey lines along the Y direction were designed to cover the entire area of the model during each measurement. In order to make each measurement start at the same position, several markers were nailed in the survey area. The three survey lines covered the area of 0.24 m to 3.6 m along the X direction. In this way, 23 CMP gathers were obtained from 0.6 m to 3.24 m with 0.12 m intervals in the cross-survey direction (X direction), and 5001 CMP gathers were obtained from 0 m to 50 m with 0.01 m intervals in the survey direction (Y direction). Overall, more than 100 thousand CMP gathers were acquired in the entire area. The B scans acquired at X=1.08 m of each survey are shown in Figure 7 (a), (b), (c), and (d), respectively. The reflection from the bottom of the level layer can be seen at approximately 0.2 m. The clear reflection around 0.5 m is the boundary of the old pavement structure. All the reflections from the level layer are mixed with the antenna coupling. From Figure 7 (b) to (d), the effect of water injection can be observed around 13 m, 31 m, and 37 m in the Y direction. However, it is hard to judge any anomalies inside the model structure through the B scans.

Figure 8 shows the CMP gather at a point in Area I along the survey line X equal to 1.08m for each of the four surveys. There is a strong difference between the first indication of arrival before and after the injection of water. But the difference with the loading test is hard to compare. The dielectric coefficient of asphalt is around 4. In this paper, we select 0.15m/ns as the propagation velocity of the pavement model. Considering the velocity of the pavement material, the reflection signals from 0 to 4 ns were used for further processing. After the entire collection of CMP gathers were processed by the proposed method, the mean wavelet entropy distribution of the entire area was acquired, as shown in Figure 9. Figure 9 (a) shows that the mean wavelet entropy value is around 0 in the entire area. But the contour of buried nonwoven fabrics (red square in Figure 9 (a)) still can be observed and matched with Figure 5 very well. In

Figure 9 (b), after several days of water injection and load test, it can clearly see that the average wavelet entropy increases significantly in the area that contained the buried nonwoven fabrics. But this change in Area I, II, and V is not smooth, which means that the change of wavelet entropy is mainly caused by water injection. In other words, the existence of this thin layer of water induces a greater change in the process of shallow reflection than the thin layer of air. The average wavelet entropy of the whole experimental area is changing with the progress of the experiment, as shown in Figure 9 (c) and (d). Overall, the relationship of entropy value is Area I>Area V>Area II>Area IV>Area III. The average wavelet entropy of the area of the nonwoven fabric is around 0.1 with the progress of the experiment. We believe that the pavement structure should not experience large damage during the load test. But, some regions show high entropy value at the end of this test, especially a high entropy value is appearing in Area I where the base layer is constructed by gravel. This means that the base layer constructed by gravel is the weakest structure compared to the other materials. The entropy value of the region located around 1 m in the X direction and 13 m in the Y direction is greater than 0.2, two times higher than the normal nonwoven fabrics region. At this point, we can conclude that the phenomenon of interlayer debonding has occurred in that region. From the results from where no nonwoven fabrics were buried, the high entropy regions during this test are around the anomalous regions in the beginning. The anomalous regions in Figure 9 (a) means these regions are not well constructed or the material used is non-uniform. That is to say, the quality of construction and the heterogeneity of the material used both have a significant effect on its service life.

Validation by Coring

~~In order~~ to obtain more details during this test, on-site coring was performed following the acquisition of multi-static GPR data. Three core samples were drilled in Area I, where the gravel was used as the base layer. The circles with a cross marker in Figure 9 (d) and Figure 10 (a) indicate the location for coring. Figure 10 (b) shows the scenario after coring. Figure10 (c), (e) and (g) show the coring sample of #1, #2 and #3, respectively, and Figure 10 (d), (f) and (h) show the coring section of #1, #2 and #3, respectively. It can be seen that the sampling of coring from #1 is uneven and some debris remains on the surface of the section. But the coring sampling from #2 and #3 are relatively integral and the coring section surface is smooth. As a consequence, defects or anomalies occurred in the region around #1 during the 30-day test. As seen from Figure 9 (d), coring #1 is located in the high entropy region, while coring #2 and #3 are located in the relatively low entropy region. The results of the coring showed that the proposed method showed reliable and excellent efficiency in detecting the defect or anomalies of the airport pavement.

CONCLUSION

We have presented a robust strategy for anomaly detection in airport pavement with a multi-static GPR system. The main objective of this research was to detect the thin voids that occurred at the bonding region in the shallow parts of airport pavement. The existence of thin water-filled or air-filled voids can be considered an inhomogeneous layer in the structure that influences the phase stability of the reflection signals in a CMP gather. It can be expected that this form of anomaly within the layered structure can be inspected by a tiny signal phase difference. During the experiment, a multi-static GPR system was used to complete the large-scale airport pavement inspection. The antenna configuration of the system and a designed survey strategy made it possible to obtain dense CMP datasets during a common survey simultaneously. Moreover, a wavelet transform was applied to these dense CMPs to evaluate the phase details of the shallow reflection. Furthermore, the mean entropy value of each CMP was used to determine the stability of the reflection phase among surveys throughout different periods. The proposed approach to inspecting anomalous regions in an asphalt layer has been illustrated by numerous field experiments with an airport pavement model. The on-site coring results also indicate the precision of the proposed approach. The proposed approach is easier to understand and the measurement process is much simpler, allowing to implement it in real-time inspection.

REFERENCES

Alani, A. M., and F. Tosti, 2018, GPR applications in structural detailing of a major tunnel using different frequency antenna systems: Construction and Building Materials, **158**, 1111-1122.

Breysse, D., 2012, Nondestructive evaluation of concrete strength: An historical review and a new perspective by combining NDT methods: Construction and Building Materials, **33**, 139-163.

Benedetto, A., F. Tosti, L.B. Ciampoli, and F. D’amico, 2017, An overview of ground-penetrating radar signal processing techniques for road inspections: Signal processing, **132**, 201-209.

Bradford, J.H., and J.C. Deeds, 2006, Ground-penetrating radar theory and application of thin-bed offset-dependent reflectivity: Geophysics, **71**(3), K47-K57.

Dasgupta, A., S. Nath, and A. Das, 2012, Transmission line fault classification and location using wavelet entropy and neural network: Electric Power Components and Systems, **40**(15), 1676-1689.

El-Zonkoly, A.M., and H. Desouki, 2011, Wavelet entropy based algorithm for fault detection and classification in FACTS compensated transmission line: International Journal of Electrical Power & Energy Systems, **33**(8), 1368-1374.

Eskelinen, P., and T. Pellinen, 2018, Comparison of different radar technologies and frequencies for road pavement evaluation: Construction and Building Materials, **164**, 888-898.

Frederickson, H.G., and T.R. LaPorte, 2002, Airport security, high reliability, and the problem of rationality: Public Administration Review, **62**, 33-43.

Fwa, T.F., 2003, Highway and airport pavement design. The civil engineering handbook.

Gerhards, H., U. Wollschläger, Q. Yu, P. Schiwek, X. Pan, and K. Roth, 2008, Continuous and simultaneous measurement of reflector depth and average soil-water content with multichannel ground-penetrating radar: Geophysics, **73**(4), J15-J23.

Hartikainen, A., T. Pellinen, E. Huuskonen-Snicker, and P. Eskelinen, 2018, Algorithm to process the stepped frequency radar signal for a thin road surface application: Construction and Building Materials, **158**, 1090-1098.

Jol, H.M., 2008, Ground penetrating radar theory and applications: Elsevier.

Jaselskis, E.J., J. Grigas, and A. Brilingas, 2003, Dielectric properties of asphalt pavement: Journal of materials in civil engineering, **15**(5), 427-434.

Kumar, P., and E. Foufoula-Georgiou, 1997, Wavelet analysis for geophysical applications: Reviews of geophysics, **35**(4), 385-412.

Kikuta, K., L. Yi, L. Zou, and M. Sato, 2019, Robust Subsurface Velocity Change Detection Method with Yakumo Multistatic GPR System: IEEE International Geoscience and Remote Sensing Symposium - IGARSS 2019.

Liu, H., C. Lin, J. Cui, L. Fan, X. Xie, and B.F. Spencer, 2020, Automatic Detection and Localization of Rebar in Concrete by Deep Learning Using Ground Penetrating Radar: Automation in Construction, **118**(10), 103279.

Liu, H., H. Lu, J. Lin, F. Han, C. Liu, J. Cui, and B.F. Spencer, 2020, Penetration Properties of Ground Penetrating Radar Waves through Rebar Grids: IEEE Geoscience and Remote Sensing Letters (early access).

Liu, H., L. Zou, K. Takahashi, M. Sato, and J. Chen, 2013, Development of an Array GPR System for Large-scale Archaeological Investigations: 11th SEGJ International Symposium – SEGJ2013

Lai, W.W.L., X. Derobert, and P. Annan, 2018, A review of Ground Penetrating Radar application in civil engineering: A 30-year journey from Locating and Testing to Imaging and Diagnosis: NDT & E International, **96**, 58-78.

Lai, W.L., T. Kind, and H. Wiggenhauser, 2011, Frequency-dependent dispersion of high-frequency ground penetrating radar wave in concrete: NDT & E International, **44**(3), 267-273.

Rosso, O.A., S. Blanco, J. Yordanova, V. Kolev, A. Figliola, M. Schürmann, and E. Başar, 2001, Wavelet entropy: a new tool for analysis of short duration brain electrical signals: Journal of neuroscience methods, **105**(1), 65-75.

Sato, M., L. Yi, Y. Itsuka, L. Zou, and K. Takahashi, 2016, Optimization of antenna polarization of the multistatic GPR system “Yakumo”: 16th International Conference on Ground Penetrating Radar – GPR2016.

Sinha, S., P.S. Routh, P.D. Anno, and J.P. Castagna, 2005, Spectral decomposition of seismic data with continuous-wavelet transform: Geophysics, **70**(6), P19-P25.

Saarenketo, T., and T. Scullion, 2000, Road evaluation with ground penetrating radar: Journal of applied geophysics, **43**(2-4), 119-138.

Shang, J.Q., and J.A. Umana, 1999, Dielectric constant and relaxation time of asphalt pavement materials: Journal of infrastructure systems, **5**(4), 135-142.

Spagnolini, U., and V. Rampa, 1999, Multitarget detection/tracking for monostatic ground penetrating radar: Application to pavement profiling: IEEE Transactions on Geoscience and Remote sensing, **37**(1), 383-394.

Shangguan, P., I. Al-Qadi, A. Coenen, and S. Zhao, 2016, Algorithm development for the application of ground-penetrating radar on asphalt pavement compaction monitoring: International Journal of Pavement Engineering, **17**(3), 189-200.

Xu, X., E.L. Miller, C.M. Rappaport, and G.D. Sower, 2002, Statistical method to detect subsurface objects using array ground-penetrating radar data: IEEE Transactions on Geoscience and Remote Sensing, **40**(4), 963-976.

Yi, L., L. Zou, K. Takahashi, and M. Sato, 2018, High-Resolution Velocity Analysis Method Using the ℓ-1 Norm Regularized Least-Squares Method for Pavement

Inspection: IEEE Journal of Selected Topics in Applied Earth Observations and Remote Sensing, **11**(3),1005-1015.

Yi, L., L. Zou, and M. Sato, 2018, Practical Approach for High-Resolution Airport Pavement Inspection with the Yakumo Multistatic Array Ground-Penetrating Radar System: Sensor, **18**(8), 2684

Yi, L., L. Zou, and M. Sato, 2018, A simplified velocity estimation method for monitoring the damaged pavement by a multistatic GPR system YAKUMO: 17th International Conference on Ground Penetrating Radar – GPR2018.

Zhang, X., N. Feng, Y. Wang, and Y. Shen, 2015, Acoustic emission detection of rail defect based on wavelet transform and Shannon entropy: Journal of Sound and Vibration, **339**, 419-432.

Zou, L., K. Kikuta, and M. Sato, 2018, Nondestructive Inspection of an Airport Pavement by MIMO Array GPR YAKUMO: 17th International Conference on Ground Penetrating Radar – GPR2018.

Zou, L., L. Yi, and M. Sato, 2020, On the Use of Lateral Wave for the Interlayer Debonding Detecting in an Asphalt Airport Pavement Using a Multistatic GPR System: IEEE Transaction on Geoscience and Remote Sensing, **58**(6), 4215 - 4224.

Zou, L., Y. Wang, I. Giannakis, F. Tosti, A.M. Alani, and M. Sato, 2020, Mapping and assessment of tree roots using ground penetrating radar with low-cost GPS. Remote Sensing: **12**(8), 1300.

LIST OF FIGURES

LIST OF TABLES

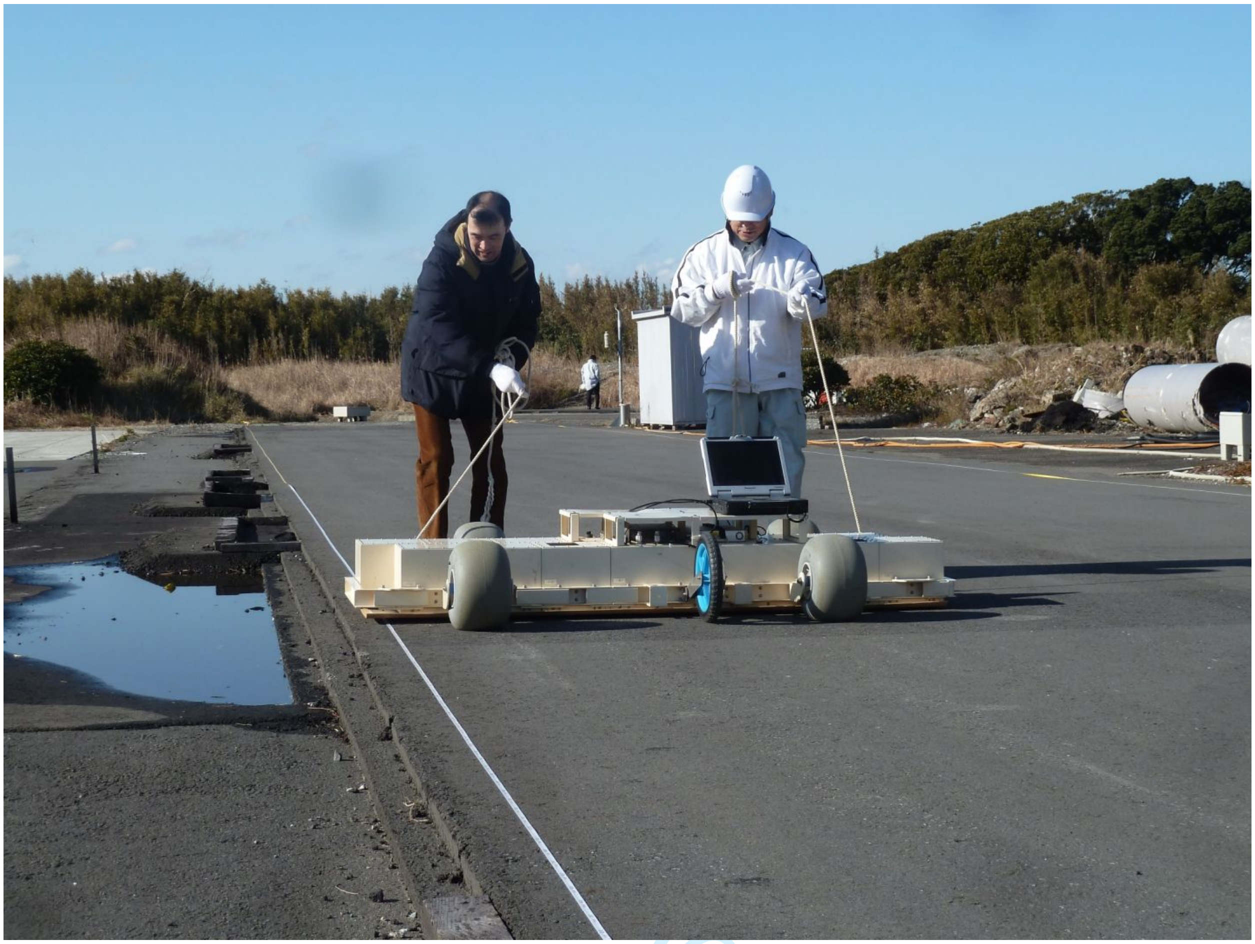

Figure 1. Multi-static ground penetrating radar system.

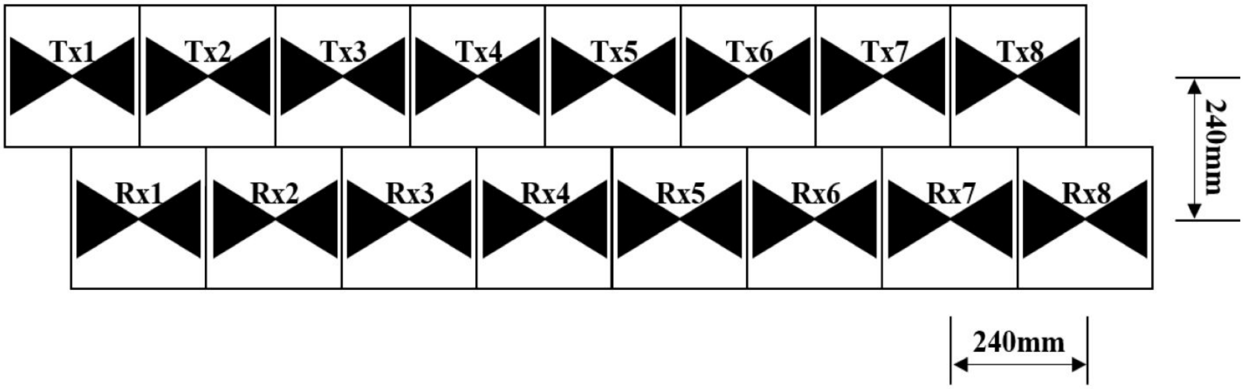

502
503
504 Figure 2. Antenna configuration of the multi-static ground penetrating radar system.

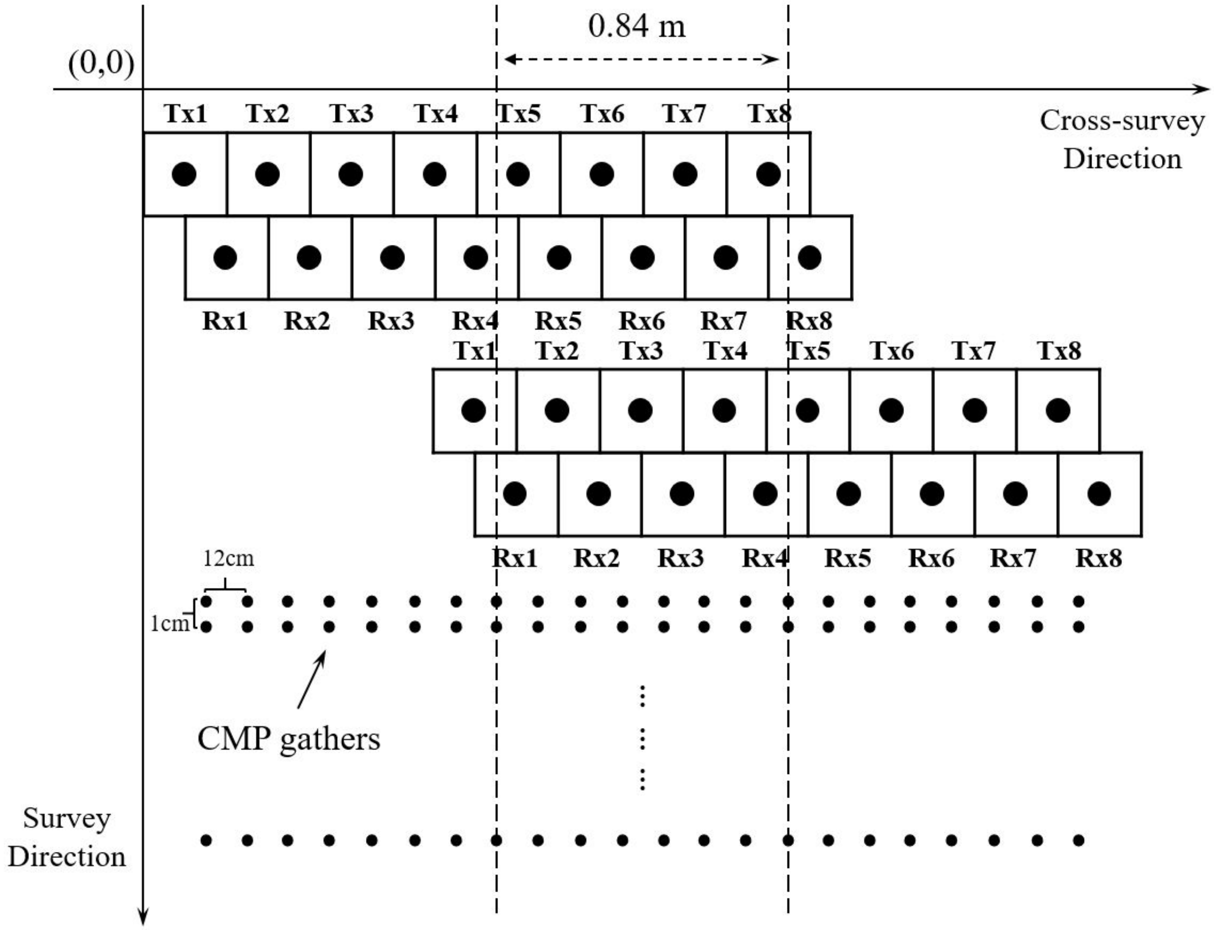

Figure 3. Measurement survey coordinate aimed for dense CMP gathers extraction.

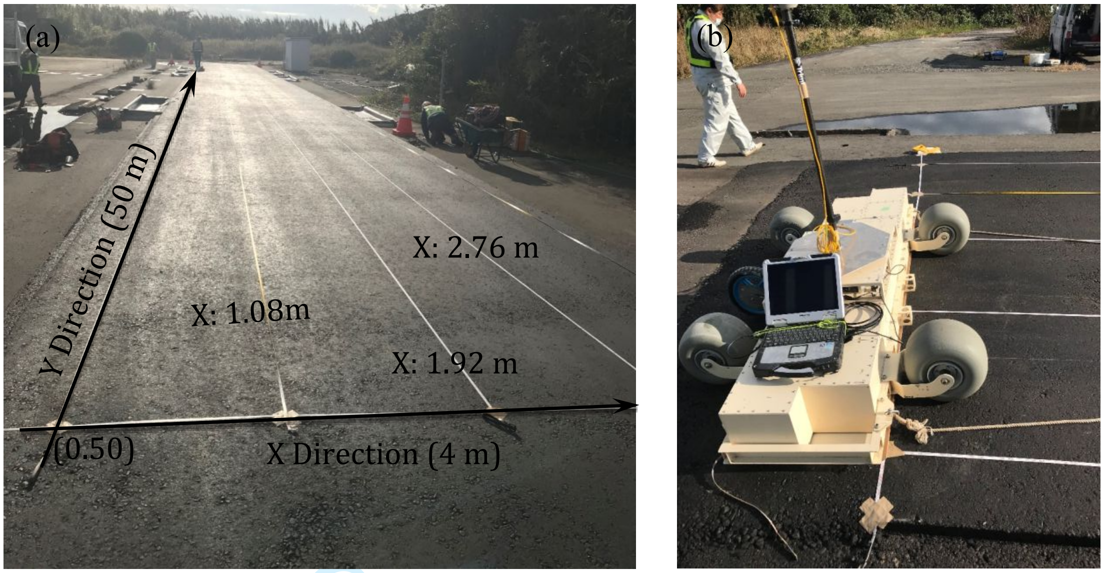

Figure 4. Measurement on the airport pavement model: (a) Entire measurement site and survey coordinate; (b) Operation of the multistatic GPR system on the site.

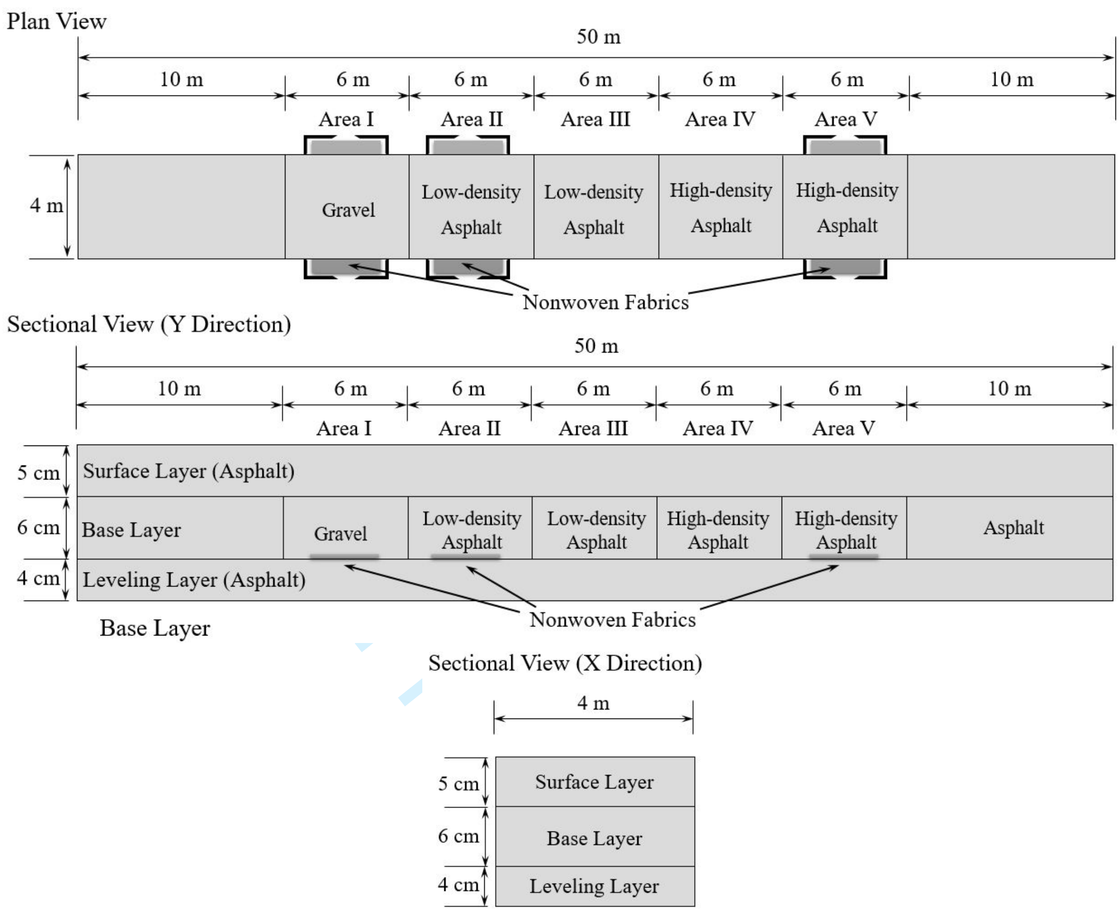

Figure 5. Structure layout of the airport pavement model (plan view and sectional view (X and Y Direction)).

Figure 6. Airport pavement model; (a) scene of Area I; (b) scene of Area II; (c) scene of Area III; (d) scene of Area IV; (e) scene of Area V; (f) the gravel base layer; (g) the hot asphalt base layer; (h)20 tons truck drove over the model to imitate the loads imposed by the aircraft.

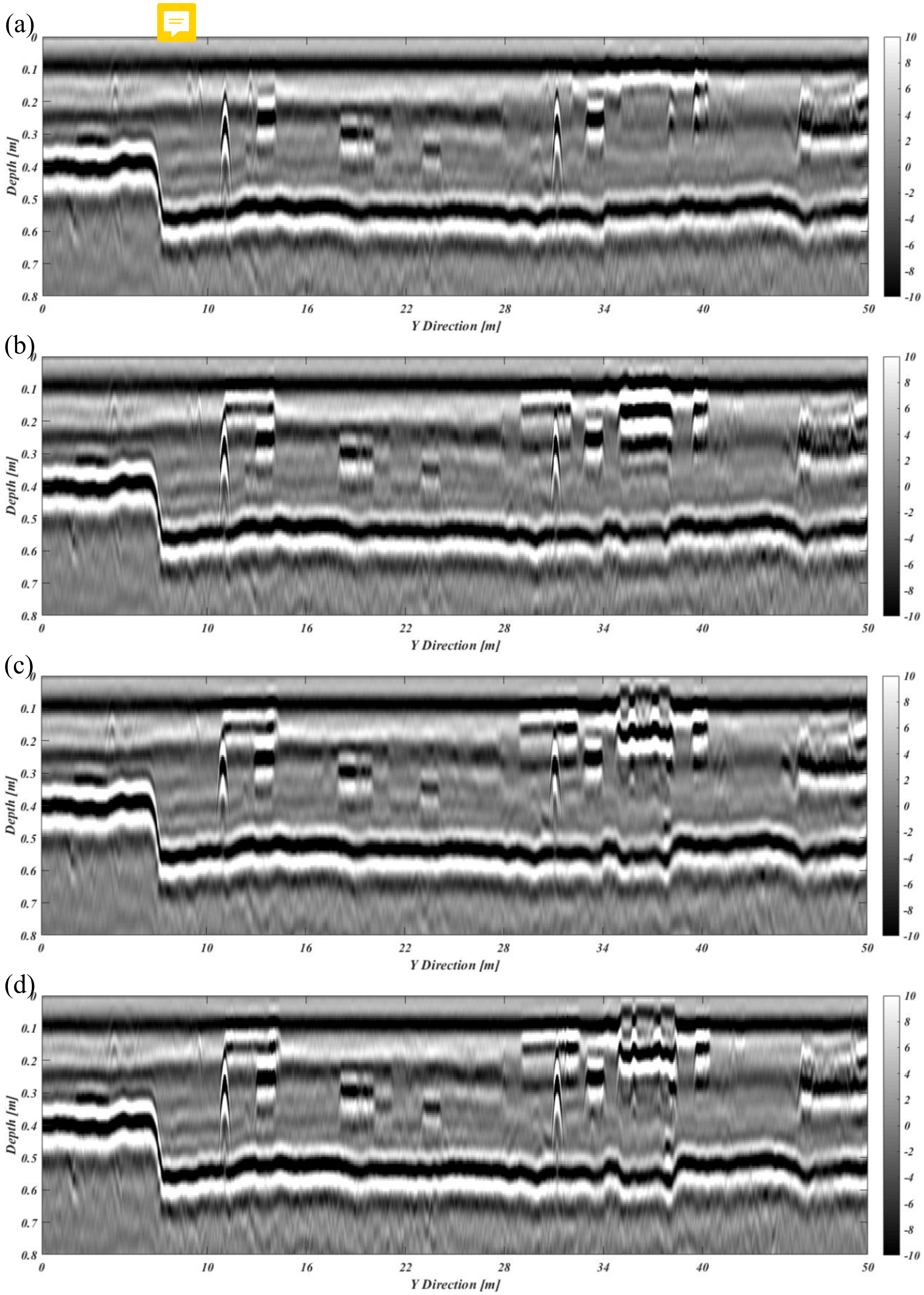

Figure 7. B scans acquired on the survey line X = 1.08m; (a) survey on 30th October; (b) survey on 6th November; (d) survey on 14th November; (d) survey on 30th November.

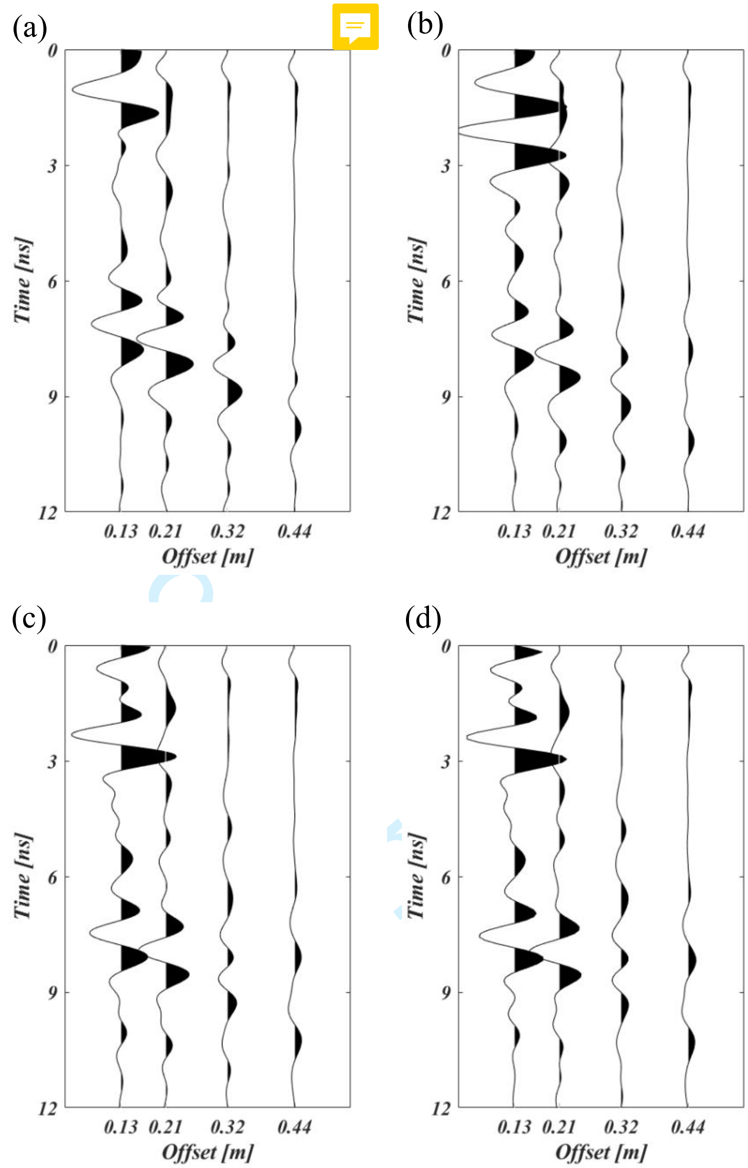

Figure 8. CMP gathers acquired at the point X = 1.08m and Y= 13m; (a) survey on 30th October; (b) survey on 6th November; (d) survey on 14th November; (d) survey on 30th November.

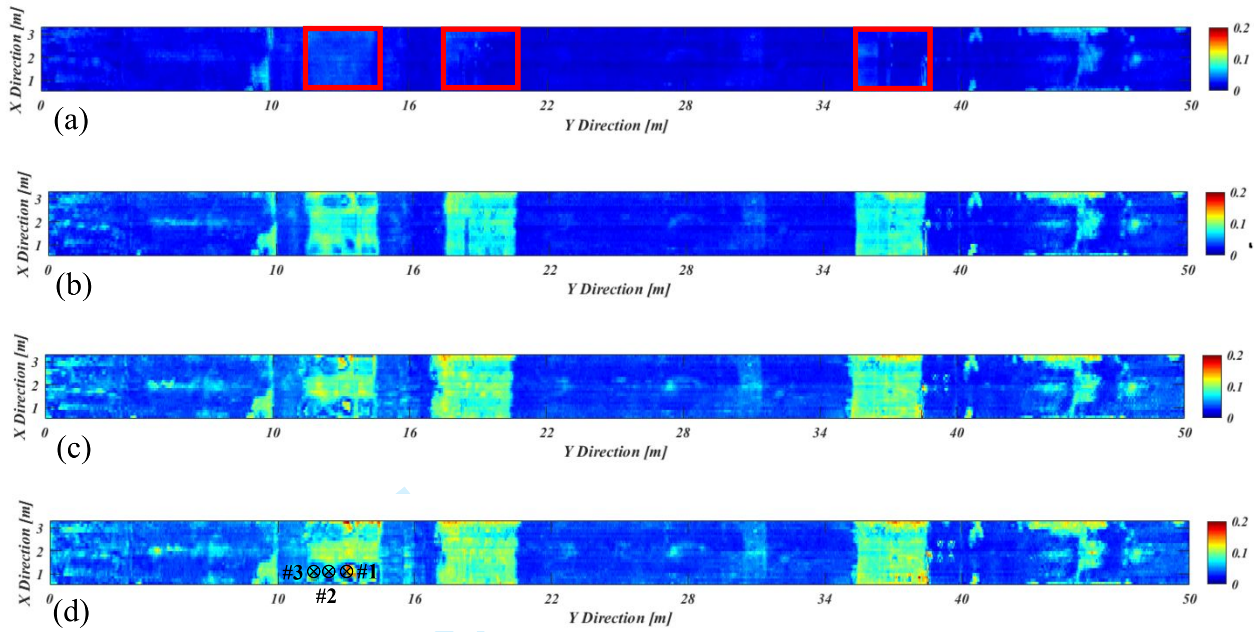

Figure 9. Mean wavelet entropy maps of the entire model: (a) entropy map of the survey on October 30th; (b) entropy map of the survey on November 6th; (c) entropy map of the survey on November 14th;(d) entropy map of the survey on November 30th.

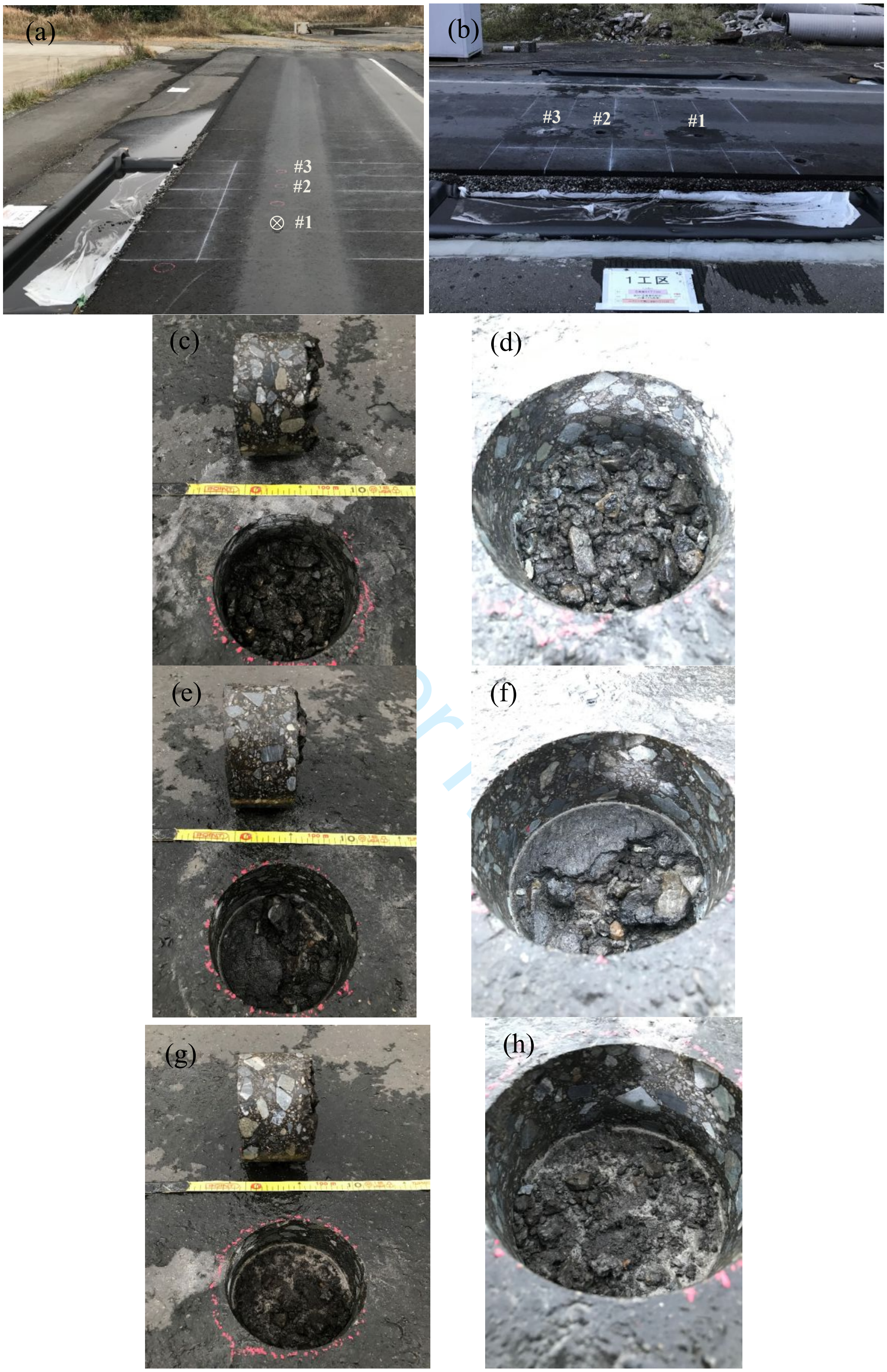

Figure 10. Coring on the pavement model in Area I: (a) #1, #2 and #3 indicated the coring position; (b) scenario after coring; (c) coring sample of #1; (d) coring section of #1; (e) coring sample of #2; (f) coring section of #2; (g) coring sample of #3; (h) coring section of #3.

parameters	values
system type	step frequency continues wave
antenna type	bowtie antenna
frequency range	0.05 GHz to 1.5 GHz
acquisition points	256
maximum movement speed	2 m/s
system width	2 m
acquisition interval	0.01 m/trace
penetration depth	larger than 2m
sweeping time	around 0.1 s

Table 1: System Parameters of the multi-static ground penetrating radar system.